Click Here for Full Article

Freshwater composition of the waters off southeast Greenland and their link to the Arctic Ocean

David A. Sutherland,[1] Robert S. Pickart,[2] E. Peter Jones,[3] Kumiko Azetsu-Scott,[3] A. Jane Eert,[4] and Jón Ólafsson[5]

[1] The freshwater composition of waters on the southeast Greenland shelf and slope are described using a set of high-resolution transects occupied in summer 2004, which included hydrographic, velocity, nutrient, and chemical tracer measurements. The nutrient and tracer data are used to quantify the fractions of Pacific Water, sea ice melt, and meteoric water present in the upper layers of the East Greenland Current (EGC) and East Greenland Coastal Current (EGCC). The EGC/EGCC system dominates the circulation of this region and strongly influences the observed distribution of the three freshwater types. Sea ice melt and meteoric water fractions are surface intensified, reflecting their sources, and generally increase southward from Denmark Strait to Cape Farewell, as well as shoreward. Significant fractions of Pacific Water are found in the subsurface layers of the EGCC, supporting the idea that this inner shelf branch is directly linked to the EGC and thus to the Arctic Ocean. A set of historical sections is examined to investigate the variability of Pacific Water content in the EGC and EGCC from 1984 to 2004 in the vicinity of Denmark Strait. The fraction of Pacific Water increased substantially in the late 1990s and subsequently declined to low levels in 2002 and 2004, mirroring the reduction in Pacific Water content reported previously at Fram Strait. This variability is found to correlate significantly with the Arctic Oscillation index, lagged by 9 years, suggesting that the Arctic Ocean circulation patterns bring varying amounts of Pacific Water to the North Atlantic via the EGC/EGCC.

1. Introduction

[2] Low-salinity waters exit the Arctic Ocean in two locations: through the west side of Fram Strait in the East Greenland Current (EGC), and through several small channels and straits of the Canadian Arctic Archipelago. Although more is known about the former pathway, basic questions still remain about the EGC and its link between the Arctic Ocean circulation and the subpolar North Atlantic to the south. For example, recent observations along the southeast coast of Greenland have revealed a separate branch of the EGC called the East Greenland Coastal Current, EGCC [*Bacon et al.*, 2002; *Sutherland and Pickart*, 2008], which is located inshore of the shelfbreak and advects freshwater equatorward. Presently it is unknown where the EGCC forms, whether it exists year-round, and what fraction of the current is due to local (e.g., runoff) versus remote (e.g., the Arctic) sources.

[3] The majority of observations to date of the EGCC are from the summer months, which has limited our understanding of its seasonality and its relationship to the EGC. Nonetheless, hydrographic and velocity data from a series of cruises from 2001–2004 have provided a basic description of the current. The EGCC is characterized by a wedge of low salinity water adjacent to the coast ($S < 34$), which supports an equatorward jet with velocities as strong as 1 m s^{-1}. The current is approximately 20 km wide, and its spatial scales agree qualitatively with coastal current theory based on midlatitude river plumes [*Sutherland and Pickart*, 2008; *Lentz and Largier*, 2006]. Using data from an extensive survey of the inner shelf in summer 2004, *Sutherland and Pickart* [2008] constructed a volume budget, which when adjusted for the effects of along-shelf wind-forcing, indicated that the combined transport of the undisturbed EGC/EGCC system is approximately 2 Sv. A rough freshwater budget of the region implied that sea ice melt was the biggest contributor to the increased freshwater flux as the current progresses southward.

[1]MIT/WHOI Joint Program, Woods Hole, Massachussetts, USA.
[2]Department of Physical Oceanography, Woods Hole Oceanographic Institution, Woods Hole, Massachussetts, USA.
[3]Bedford Institute of Oceanography, Dartmouth, Nova Scotia, Canada.
[4]Oceanografix, Victoria, British Columbia, Canada.
[5]University of Iceland and Marine Research Institute, Reykjavik, Iceland.
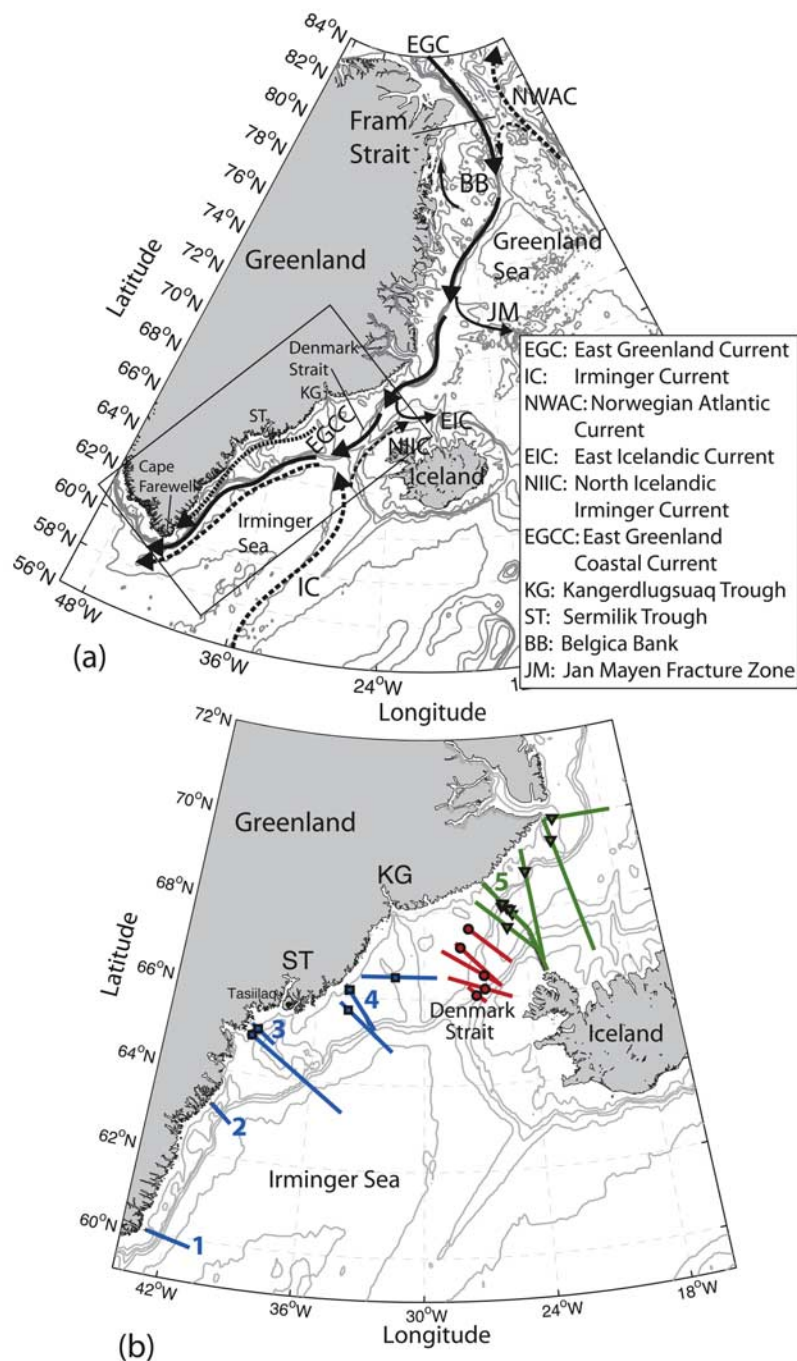
Figure 1. (a) Surface circulation schematic for the northern North Atlantic showing the dominant freshwater pathways from the Arctic (solid lines) and the Atlantic-origin waters (dashed lines). (b) Locations of the JR105 sections (1–5) occupied in 2004. Historical sections are also shown, color coded by their proximity to Denmark Strait (Table 4). Markers indicate the position of the EGC or EGCC current core. The 200, 400, 1000, 2000, and 3000 m isobaths are shown in light gray [*IOC et al.*, 2003].

[4] *Bacon et al.* [2002] suggested that the EGCC might be formed mainly as a result of meltwater and runoff from the Greenland continent. The more extensive data set noted above, analyzed by *Sutherland and Pickart* [2008], suggests that the main part of the flow originates from a bifurcation of the EGC south of Denmark Strait (although modification by meltwater is certainly present). In particular, when the EGC encounters the Kangerdlugssuaq Trough (KG, Figure 1), a portion of the flow is diverted onshore and continues equatorward along the inner shelf. There is evidence from a set of recent laboratory experiments that this is a time-dependent process that depends on the strength and spatial scales of the EGC as it encounters the KG trough [*Sutherland and Cenedese*, 2008]. A similar diversion of water from the

shelfbreak to the inner shelf seems to occur farther south as well, associated with the deep canyon near 65.5°N, 38°W called the Sermilik Trough (Figure 1). This is suggested from water mass considerations [*Sutherland and Pickart*, 2008] as well from previous drifter studies [e.g., *Bacon et al.*, 2002; *Centurioni and Gould*, 2004].

[5] The results from the cruises over the last half-decade, together with the historical data analysis by *Wilkinson and Bacon* [2005], indicate that the EGCC is a persistent feature in summertime. There is evidence as well that the current is present year-round. *Malmberg et al.* [1967] reported on data from a short mooring deployment on the shelf near 66°N suggesting that an inner shelf flow was present outside of summer, though they identified it as the EGC. Also, several surface drifters released in the winter of 2000 north of Denmark Strait followed the EGC initially [*Bacon et al.*, 2008], but in the northern strait one of them moved onto the shelf and was advected southward by the EGCC (there was a high level of variability most likely caused by the strong winter winds).

[6] Since the EGCC appears to be a branch of the EGC (i.e., it is not simply the result of coastal runoff) and may be present year-round, it likely has a link to the Arctic Ocean. Hence the EGC/EGCC system offers a useful place to examine interannual variations in freshwater entering the North Atlantic from the Arctic. Knowledge of the freshwater composition of the EGCC is valuable in understanding its origins, any long-term changes observed in the future, and to aid in the interpretation of freshwater budgets calculated for the region [*Sutherland and Pickart*, 2008] or for the pan-Arctic system [e.g., *Dickson et al.*, 2007; *Serreze et al.*, 2006].

[7] In the Arctic system, *Steele et al.* [2004] suggested that Pacific Water pathways might shift under different circulation regimes; these regimes have been shown to be related to the Arctic Oscillation (AO) [*Proshutinsky and Johnson*, 1997]. This in turn implies that there may be an associated interannual pattern in the freshwater concentrations of the EGC/EGCC. Attempts to relate Pacific Water content of the EGC to changing Arctic Ocean circulation patterns have thus far been inconclusive, however. While significant interannual variability of Pacific Water in the EGC has been observed in the vicinity of Fram Strait [*Jones et al.*, 2003; *Taylor et al.*, 2003; *Falck et al.*, 2005], no relationship to the AO has been found. For example, *Falck et al.* [2005] showed a dramatic diminishment of Pacific Water content near Fram Strait between 1997 and 2004, but could not relate it to the AO since it was based on only four sections taken between 1984 and 2004.

[8] The primary goals of the present study are as follows. First, we wish to elucidate the freshwater composition of the EGCC in order to understand better its relationship to the EGC and hence the Arctic Ocean. Second, we aim to quantify the interannual variation of Pacific Water in the EGC/EGCC along southeast Greenland, and relate this to time varying export pathways from the Arctic Ocean. We apply a suite of methods that have been used previously in the literature, mostly based on tracer techniques [e.g., *Östlund and Hut*, 1984; *Schlosser et al.*, 1994; *Bauch et al.*, 1995; *Jones et al.*, 1998]. These methods are used to calculate the percentages of Pacific Water, Atlantic Water, sea ice melt, and meteoric water, based upon measurements

of dissolved nutrients (nitrate and phosphate in particular), oxygen isotopes, salinity, and alkalinity. After examining the EGCC using data from the summer 2004 survey noted above, a compilation of historical hydrographic/tracer sections from the vicinity of Denmark Strait are analyzed to investigate interannual variation of Pacific Water content in the EGC/EGCC from 1984 to 2004. This is subsequently interpreted in light of shifting patterns in the AO.

2. Data and Methods

2.1. Data and Sample Acquisition

[9] The primary source of data for this study comes from a July–August 2004 cruise on the ice-strengthened vessel *RRS James Clark Ross* (JR105) along the numbered transects shown in Figure 1. A total of 156 hydrographic stations comprising five cross-shelf sections were occupied using a Seabird 911+ conductivity/temperature/depth (CTD) system. Water to measure dissolved oxygen, salinity, and nutrient concentrations was obtained with a 12×10 liter bottle rosette. We used the salinity bottle samples to calibrate the CTD conductivity sensor. Measurement accuracies are 0.002 for salinity and 0.001°C for the temperature sensor.

[10] A key advantage of this data set is the high-resolution cross-stream station spacing and the relatively close proximity to the coast of each inshore station (both on the order of 5 km). This represents the first oceanographic data of its kind for the southeast Greenland inner shelf between Denmark Strait and Cape Farewell. The processing and analysis of the CTD station data, consisting of salinity and temperature, were discussed in detail by *Sutherland and Pickart* [2008], along with direct velocity measurements obtained with a narrow band, 150 kHz vessel-mounted acoustic Doppler current profiler (ADCP) that ran continuously during the cruise.

[11] Nutrients, including nitrate (NO_3), phosphate (PO_4), and silicate (SiO_4), were analyzed on board in duplicate from the bottle samples. The analysis procedure followed the World Ocean Circulation Experiment (WOCE) protocol using a Technicon Autoanalyzer, with precisions close to 1% [*Gordon et al.*, 1993]. Bottle depths were spaced ~25 m apart in shallow water over the shelf (bottom depth < 200 m), while in deeper waters the sample resolution ranged from 100 to 200 m. Water samples for the determination of oxygen isotope and alkalinity were collected from bottles and analyzed later at the Bedford Institute of Oceanography. Oxygen isotope composition was measured by an equilibrium technique using Micromass Isoprime™ with double injection (two-tier inlet) coupled with an Aquaprep™ system. Data are reported with respect to standard mean ocean water (SMOW) in the $\delta^{18}O$ notation (per mil deviation) with analytical precision of $\pm 0.03–0.05$‰. An automated open-cell potentiometric titration system was used to determine alkalinity. Alkalinity measurements were calibrated with Certified Reference Material (CRM, Scripps Institution of Oceanography) and the analytical precision was $\pm 4–5$ μmol kg^{-1}.

[12] The sampling for oxygen isotope was less frequent than for nutrients, with all of the isotope data derived from bottles shallower than 60 m and at a lower horizontal resolution (i.e., not every station). Less frequent still were samples for alkalinity, which were taken at only 1–2 stations
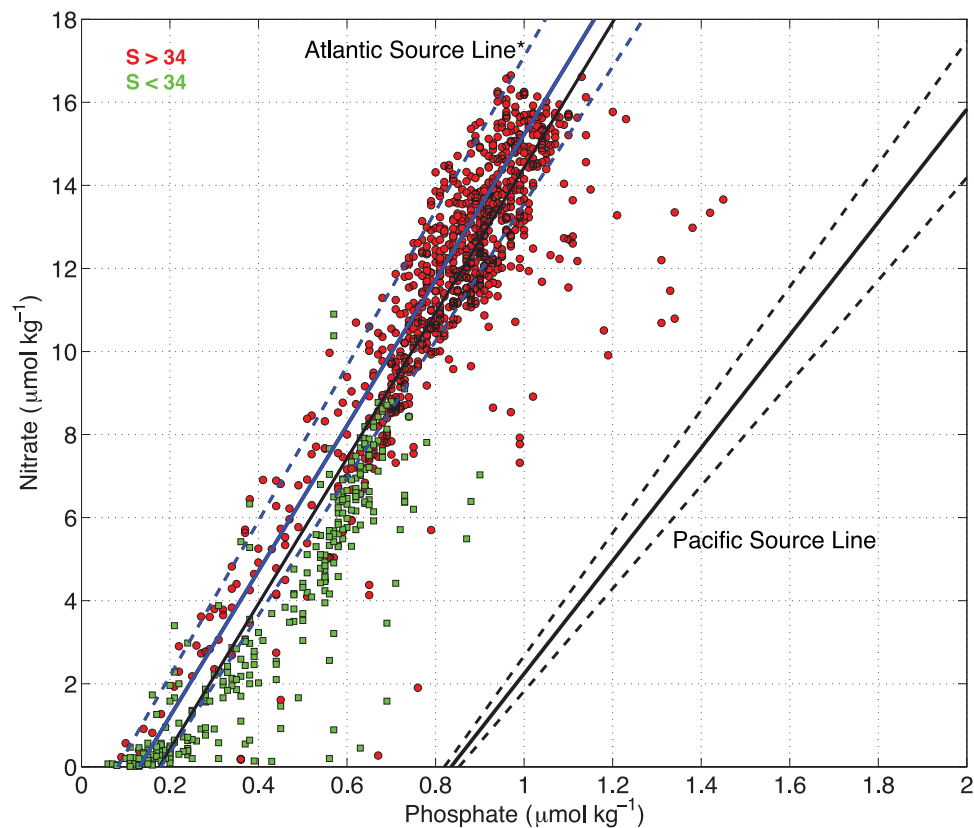
Figure 2. Phosphate versus nitrate values for data collected during JR105 in 2004, separated into low-salinity waters ($S < 34$, green squares) and the remaining data (red circles). Solid lines are fits to Atlantic* and Pacific source waters with their expected error bounds shown as dashed lines (see text). The source lines of *Jones et al.* [2003] are shown in black, while the AW source line from the JR105 data is in blue.

per transect, but were spaced vertically throughout the water column. The effects of these sampling schemes on the results below are minimal. In particular, since $\delta^{18}O$ distinguishes water of meteoric origin, such as precipitation or runoff, from that of sea ice origin, its utility is limited to the upper water column and the results discussed below seem to capture all the freshwater of meteoric origin. Also, in the present study alkalinity is used as a separate tracer only in place of $\delta^{18}O$, in order to assess the sensitivity of the freshwater decomposition results to a particular method.

2.2. Quantification of Freshwater Composition

[13] The process of quantifying the freshwater fractions of a given water sample requires knowledge of the properties of the pure freshwater contributions. In Arctic Ocean waters, these sources include the major rivers that drain into the basin, the inflow from the Pacific Ocean through Bering Strait, sea ice melt, water entering through Fram Strait and the Barents and Kara Seas, and precipitation. Previous studies have used chemical tracers, combined with salinity data, to separate the relative proportions of each freshwater source in a water sample [e.g., *Östlund and Hut*, 1984; *Bauch et al.*, 1995; *Jones et al.*, 1998]. In particular, the works of *Jones et al.* [2008] and *Taylor et al.* [2003] combined nutrient-based techniques and chemical tracer data to examine the freshwater pathways in the Arctic and along the northeast coast of Greenland. We apply their method to southeast Greenland using data from JR105.

[14] The goal of the freshwater decomposition is to calculate the relative amounts of Pacific Water (PW), Atlantic Water (AW), sea ice melt (SIM), and meteoric water (MW), expressed as fractions. The decomposition occurs in two steps. The first is to determine the fraction of Pacific Water. We follow the work of *Jones et al.* [1998], who showed that by examining the nitrate-phosphate (N-P) relationship of a polar water sample, the relative amount of Pacific Water could be determined to within ±10%. This technique is successful because as water travels over the shallow Bering Sea shelf entering the Arctic Ocean, it is stripped of its nitrate by biological processes and mixing with nutrient-poor runoff [*Cooper et al.*, 1997; *Jones et al.*, 1998]. This means that a regression line of nitrate versus phosphate will have a different y intercept than water of Atlantic origin (the slope of the regression line is the same for both Pacific and Atlantic waters, since biological processes set the slope in Redfield ratios).

[15] Figure 2 shows the N-P relationship for the JR105 nutrient data. This method finds the percentage of PW present in a sample by drawing a mixing line between the PW and AW sources; the latter represents not only AW, but sea ice melt and meteoric waters as well, since they have N-P relationships very similar to AW [*Jones et al.*, 1998]. The data in Figure 2 with $S < 34$ are highlighted green since there was an appreciable departure of the low-salinity water during JR105 from the AW source line. The values of the y intercept and slope of the PW and AW source lines are

Table 1. End-Member Values (and Their Uncertainties) Used in Calculating the Pacific Water Fraction f_{PW}

	Atlantic Water	Pacific Water
NO$_3$/PO$_4$ slope	20.7 (±1.4)	12.4 (±2.4)
NO$_3$/PO$_4$ intercept	−2.70 (±1.0)	−10.5 (±1.6)

Table 2. End-Member Values (and Their Uncertainties) Used in the Freshwater Composition Calculation[a]

	Atlantic Water	Pacific Water	Sea Ice Melt	Meteoric Water
Salinity	35 (±0.15)	32.7 (±1)	4 (±1)	0
δ^{18}O (‰)	0.35 (±0.1)	−1 (±0.1)	1 (±0.5)	−21 (±2)
Alkalinity (μmol kg^{-1})	2296 (±20)	2170 (±20)	263 (±20)	1000 (+400)

[a]δ^{18}O is relative to standard mean ocean water (SMOW).

listed in Table 1. The AW source line is calculated from the JR105 data using the nutrient values of water with $S > 35$ (blue line in Figure 2), while the other source lines come from previous studies. In particular, a second AW source line is derived from data entering the Arctic Ocean via the St. Anna Trough in the Kara Sea (black line in Figure 2), which is assumed to be representative of pure Atlantic Water. The PW source line comes from data sampled in the Chukchi Sea of the Arctic Ocean, a primary pathway for the Pacific Ocean inflow through Bering Strait. Figure 2 demonstrates that the AW sources from the Irminger Sea and the Kara Sea (which would return to the North Atlantic via the EGC as modified AW) are not measurably different in their N-P relationship.

[16] In practice, the fraction of PW, f_{PW}, is calculated using

$$f_{PW} = \frac{PO_4^m - PO_4^{AW*}}{PO_4^{PW} - PO_4^{AW*}} \quad (1)$$

where PO_4^m is the measured phosphate value, PO_4^{PW} is the phosphate value the sample would have if it was purely Pacific Water (i.e., on the PW source line in Figure 2), and PO_4^{AW*} is the phosphate value the sample would have if it was Atlantic source water. The star indicates that this Atlantic source water also includes the SIM and MW fractions, since their nutrient relationships are similar.

[17] The second step in determining the freshwater composition of a water parcel is to differentiate between the AW, SIM, and MW contributions, once f_{PW} is known. This is accomplished using the following set of conservation equations

$$f_{AW} + f_{SIM} + f_{MW} = 1 - f_{PW} \quad (2)$$

$$O_{AW}^{18}f_{AW} + O_{SIM}^{18}f_{SIM} + O_{MW}^{18}f_{MW} = O_m^{18} - O_{PW}^{18}f_{PW} \quad (3)$$

$$S_{AW}f_{AW} + S_{SIM}f_{SIM} + S_{MW}f_{MW} = S_m - S_{PW}f_{PW} \quad (4)$$

for mass (equation (2)), salinity (equation (3)), and oxygen isotope (equation (4)), where $O^{18}{}_m$ and S_m are the observed values and f_{SIM}, f_{MW}, and f_{AW} are the relative fractions of the three unknown water types: sea-ice meltwater, meteoric water, and Atlantic Water. The end-member values multiplying the fractions, f, are listed in Table 2.

[18] High-latitude waters of meteoric origins are isotopically light compared to their oceanic counterparts, which makes oxygen isotope data useful as a tracer. Ranges of δ^{18}O values in Arctic rivers, for instance, are −13.3 to −23.8‰ [Ekwurzel et al., 2001]. Figure 3a illustrates this

by showing the δ^{18}O-S relationship for the JR105 data, where any water with a significant fraction of MW will be along a mixing line between oceanic water (OW), which in this case includes both AW and PW, and pure MW. The JR105 data show some influence of meteoric water, as well as some influence of sea ice melting and freezing, which
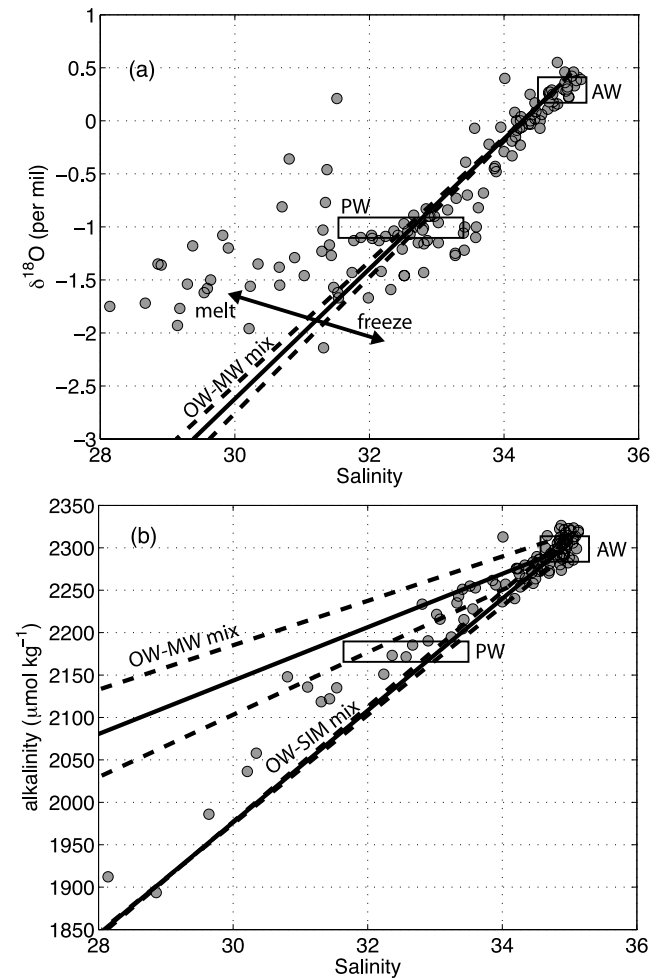

Figure 3. (a) δ^{18}O versus salinity for 2004 JR105 data (circles). A mixing line between oceanic water (OW) and meteoric water (MW) is shown. OW includes Atlantic Water (AW) and Pacific Water (PW), whose ranges are indicated by the boxed regions. Dashed lines show the bounds on the end-member values (Table 2), while the arrows indicate the influence of sea ice melt/formation processes. (b) Same as in Figure 3a, but for total alkalinity (μmol kg^{-1}) versus salinity.

tends to change the salinity of the water independent of its isotopic signature (Figure 3a). Uncertainties in the $\delta^{18}O$ end-member values (Table 2) result in the error bounds shown in Figure 3a.

[19] The largest uncertainties in the two-step method come in choosing the end-member values for the different source waters. Values in Tables 1 and 2 are taken from the existing literature [*Jones et al.*, 2003; *Taylor et al.*, 2003; *Ekwurzel et al.*, 2001; *Bauch et al.*, 1995] with the exception of the AW values. These are estimated from the JR105 hydrographic data set, since in the vicinity of southeast Greenland the dominant AW source is more likely to be the retroflecting Irminger Current offshore of the shelfbreak [*Pickart et al.*, 2005], than the remote waters of the Nordic or Barents Seas.

[20] For comparison we also show results using the measurements of alkalinity in place of oxygen isotope in equation (3), where possible, since alkalinity is a good indicator of meteoric water as well. This is illustrated in Figure 3b, which shows the alkalinity-salinity relationship using the JR105 data. Note that there was considerably less alkalinity data available (only 32 samples) than isotope data. However, the influences of sea ice melt and meteoric water can still be seen in the 2004 data as the measurements fall mainly along either the OW-MW or OW-SIM mixing lines, with some showing the influence of both.

3. Freshwater Composition of the EGCC

[21] A primary motivation for this study was to examine the origins of the EGCC by looking at the relative abundances of each freshwater type, determined by the tracer analyses described above. If the current was entirely driven by local runoff and ice melt, then one would not expect to see a signature of Arctic-origin water, either through the presence of PW or negative SIM fractions that suggest ice formation and an Arctic origin. We focus on the distribution of Pacific Water in the JR105 sections first, followed by a discussion of the presence of sea ice melt and meteoric water.

3.1. Pacific Water

[22] Figure 4 shows the PW fractions calculated for each JR105 transect, along with selected isohalines to help indicate the position of both the EGC and/or EGCC features. Low-salinity values correspond well with the maximum equatorward velocity and suggest the presence of the EGC/EGCC current core, which should influence where PW is observed, while the 35-isohaline illustrates the presence of the AW front.

[23] Starting with the northernmost section near 68°N (section 5, Figure 4a), significant f_{PW}s are found within the wedge of fresh water ($S < 34$), with the largest values inshore of the EGC. At this latitude, the EGC is situated well offshore in the center of Denmark Strait. There is only a weak signature of the EGCC at this northern location, with slightly enhanced equatorward flow between stations 110–114 (Figure 4a). The largest f_{PW} is approximately 0.3, and the average throughout the subsurface layer extending toward the coast is ~0.15.

[24] Note that the f_{PW}s are zero near the surface and are eroded in the core of the EGC.

[25] This reduction of PW fraction in the current core is possibly due to an increase in mixing within the jets, a notion that can be tested by looking at the bulk Richardson number, $Ri = N^2/U_z^2$, of the flow, where N is the buoyancy frequency and U_z is the vertical shear in the horizontal velocity. Values of $Ri < 0.25$ indicate the presence of strong mixing driven by shear instabilities. Calculations of Ri for the 2004 sections (not shown) suggest that mixing was strong in the EGCC. The reduction of PW in the surface layer is linked to the additional input of other freshwater components to the EGC/EGCC as it progresses southward along the Greenland shelf (see the MW and SIM discussion below, and Figures 5 and 6).

[26] Farther south at section 4 (near 66°N, Figure 1), similar distributions of f_{PW} are observed (Figure 4b). The maximum fraction of PW resides in a subsurface layer within the wedge defined by the 34-isohaline. At this latitude, the EGCC is present over the inner shelf, far inshore of the shelfbreak where the EGC usually resides. Note that there are two velocity peaks associated with the EGCC here, an indication of the EGCC's susceptibility to wind events and its small spatial scales [*Sutherland and Pickart*, 2008]. Associated with each of these separate jets is a subsurface maximum in f_{PW}, suggesting that the PW signal is being carried by the deeper part of the current. The enhanced equatorward flow near the location where the 34-isohaline outcrops ($x = 100$ km) is most likely due to an eddy that contains a mix of northern-origin PW and warm/salty AW from the Irminger Current. Flux of AW onto the shelf at this latitude is commonly observed and is likely related to the formation of eddies, possibly due to baroclinic instability of the EGC/IC [*Pickart et al.*, 2005]. Two such lenses of Irminger Current water with $S > 35$ (devoid of a PW signal) are situated near the shelf edge (Figure 4b).

[27] Section 3, located on the inshore side of the Sermilik Trough (Figure 1), shows relatively higher f_{PW} than farther north, but with a similar spatial distribution (Figure 4c). Maximum fractions are ~0.3–0.4, but within the high-speed core of the EGCC the signal is again close to zero, as it was in the main jet features sampled to the north (the EGC was not sampled at this location because the section did not extend far enough offshore). At section 2 (63°N), the shelf reaches its narrowest point, where the EGC and EGCC are thought to partially merge [*Sutherland and Pickart*, 2008]. The distribution of PW shown in Figure 4d is similar to that of section 3, except for the presence of the EGC at the shelfbreak which has significant f_{PW} to depths of 250 m. Offshore of this lies AW ($S > 35$), with no PW present.

[28] The biggest alongstream change in the f_{PW} distribution measured during JR105 occurs at section 1, off Cape Farewell near 60°N (Figure 4e), where no significant PW fractions were observed. This could be due to a strong presence of Irminger Current water and/or other freshwater components. More likely, the peak PW signal in the EGC/EGCC system was mixed away or transported offshore of the section by the strong winds that regularly occur near Cape Farewell. As reported by *Sutherland and Pickart* [2008], prior to occupying section 1 the prevailing winds were upwelling favorable. This caused the EGCC to shoal, with its surface signature extending offshore, akin to the manner in which river plumes react to upwelling winds
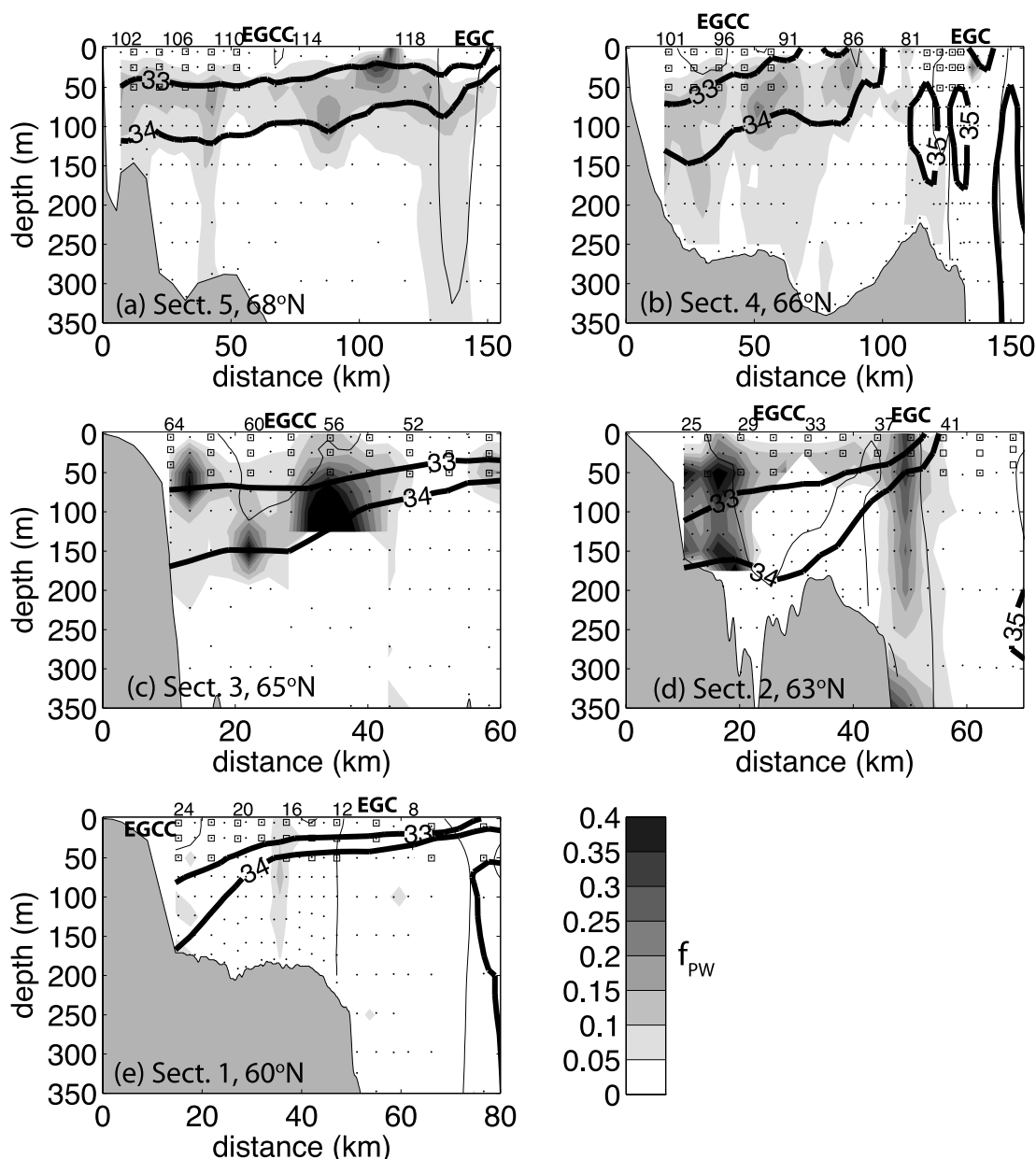
Figure 4. (a–e) Fractions of Pacific Water, f_{PW} (shading), for each JR105 section, along with the 33, 34, and 35 isohalines (thick lines). EGCC and EGC labels correspond to the location of the current core, outlined by the 30 cm s^{-1} contour of alongstream velocity (thin line). Dots indicate nutrient sample locations, while squares are isotope sample locations. Note that the horizontal scale changes between panels. The numbers along the top of each panel refer to the station number.

[e.g., *Lentz and Largier*, 2006]. This is seen in Figure 4e by the shallow 34-isohaline, which extends seaward of the shelfbreak over the AW layer. Only a small velocity signal is seen on the inshore most part of the shelf. This jet is the remnant of the EGCC after the wind event and is also partially the result of continual input of runoff (MW) and sea ice melt. The MW and SIM signals discussed below support this idea.

[29] Hence by Cape Farewell, the PW signal is lost, either due to the thinning of the surface layer and enhanced mixing driven by the strong upwelling winds, or to the movement of the PW into the basin interior beyond the extent of our transect. In summary, during the summer of

2004, the EGCC contained significant fractions of PW, which in turn implies that the current receives significant input from the Arctic-origin EGC. The PW signal was strongest in subsurface layers and reduced in the core of both the EGC and EGCC. However, the values seen near Denmark Strait (~0.2) were lower than those reported in previous years [*Jones et al.*, 2003; *Dodd*, 2007]. Whether this is due to interannual variability or just the synopticity of the sections is explored later in the paper (section 4).

3.2. Sea Ice Melt

[30] Figure 5 shows the results of the analysis for sea ice meltwater. Note that the data coverage for calculating f_{SIM}
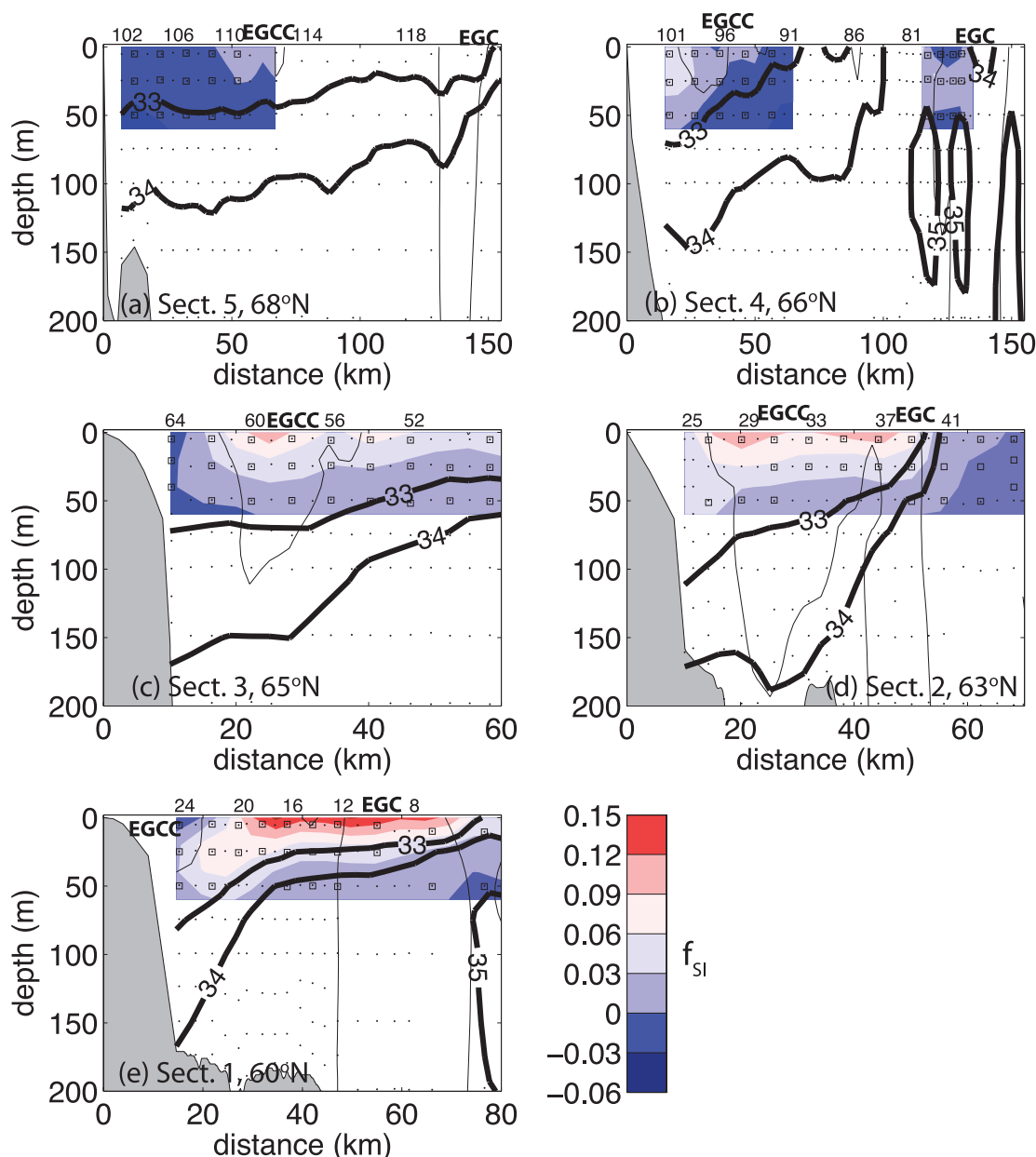
Figure 5. (a–e) Same as Figure 4, but for fractions of sea ice melt, f_{SIM} (color). Note that the vertical scale has been reduced to emphasize the upper water column in all the panels.

and f_{MW} (below) is less than the coverage for f_{PW}, since the latter calculation was based on the more frequently sampled nutrients. Squares indicate positions of isotope data, which are all shallower than 60 m. Negative fractions indicate that net sea ice formation has occurred from that water sample [*Östlund and Hut*, 1984]. Along the southeast coast of Greenland, most sea ice is advected from the north [*Cavalieri et al.*, 2005], so that any water with $f_{SIM} < 0$ is evidence of polar-origin water that underwent ice formation the previous winter.

[31] North of Denmark Strait at JR105 section 5, f_{SIM} ranged from $-.04-0$, with the most negative values observed inshore of the EGCC (Figure 5a). Based on hydrographic analysis, *Sutherland and Pickart* [2008] determined that the surface waters at this location closely resembled

Polar Surface Water (PSW), an Arctic-origin water mass modified along its journey by sea ice melt and solar heating [*Rudels et al.*, 2002]. Note that f_{SIM} increases toward zero near the core of the EGCC. Integrating over the upper 60 m and accounting for the different densities of seawater and ice, the values of f_{SIM} represent $\sim 2-3$ m of sea ice formed. Note that there was no sea ice melt observed anywhere along the section. By contrast, surface waters downstream of the Kangerdlugssuaq Trough do reveal the presence of sea ice melt (Figure 5b). f_{SIM} are positive closest to the coast, on the inshore side of the main EGCC feature, suggesting that the sea ice advected along with this current has undergone melting. Hydrographic data support this as well, as the near surface waters are warmer and fresher than at section 5 to the north. Another notable feature at section 4
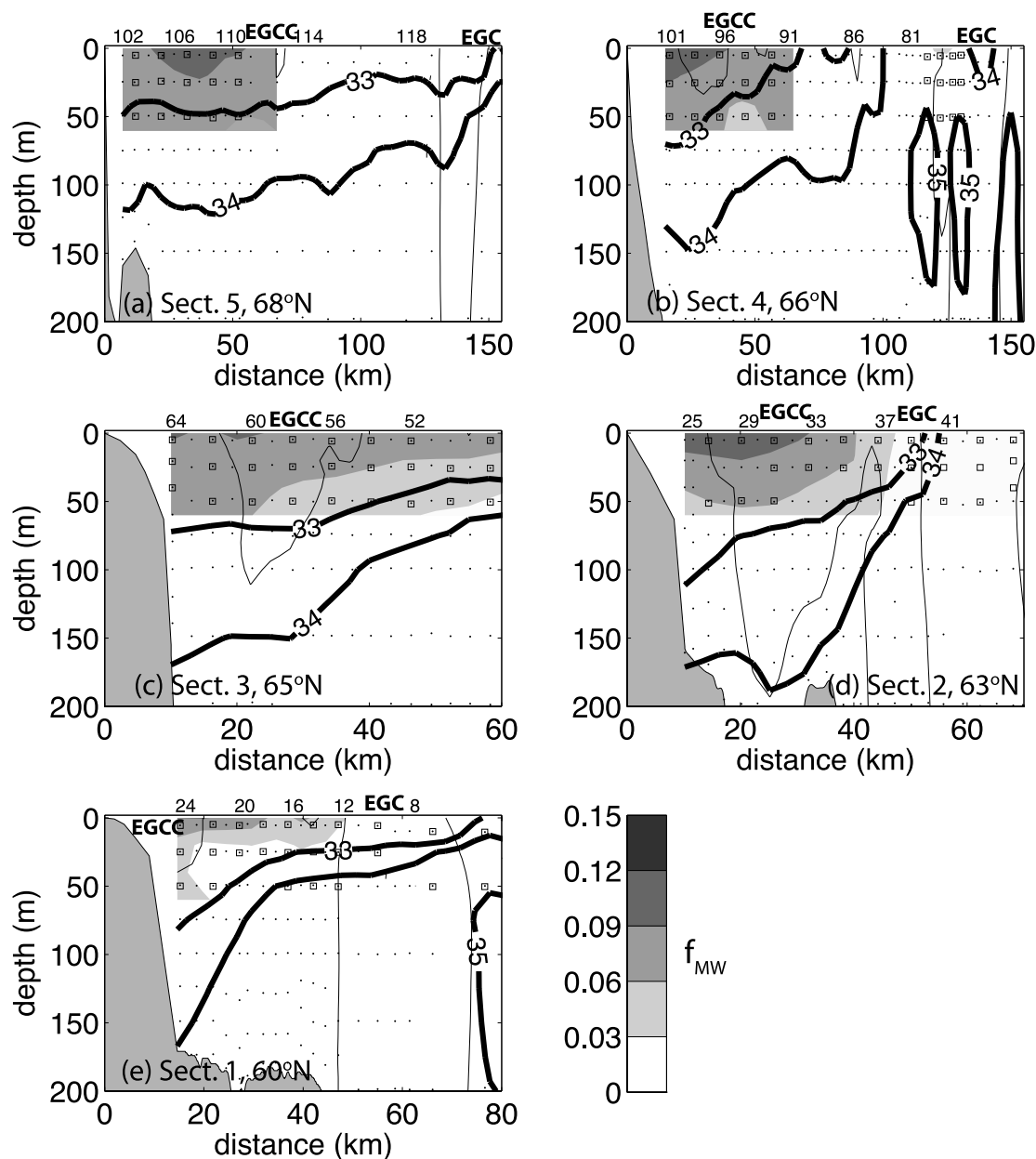
Figure 6. (a–e) Same as in Figure 5, except fractions of meteoric water, f_{MW} (shading).

are the negative f_{SIM} situated between the two salty AW lenses near the shelfbreak. This implies that the cross-shelf exchange of AW and fresher, polar-origin water is a convoluted process, with shelf water becoming intertwined with the AW filaments.

[32] Sea ice melt increases to the south over the remaining part of the southeast Greenland shelf. In sections 3 and 2 (Figures 5c and 5d), f_{SIM} values reach ~0.1, with maxima near the core of the EGCC jet and in the upper 20 m of the water column. The deeper extent of positive f_{SIM} close to the coast at section 2 is probably a result of the strong downwelling favorable winds that occurred prior to the sampling. These downwelling favorable winds act in the opposite sense of the upwelling winds described above: the current width narrows and the foot of the front deepens

as the winds accelerate the current and the Ekman-driven flow drives surface waters toward the coast [*Sutherland and Pickart*, 2008; *Lentz and Largier*, 2006]. The sea ice melt at section 1 is observed to extend far offshore (Figure 5e), likely a consequence of the upwelling winds that seem to have influenced the PW signature. Maximum f_{SIM} are ~0.12–0.15 here, but with no significant levels found within the EGCC near $x = 15$ km. Visual observations during the time of the cruise support this cross-shelf distribution, with floating ice observed far offshore of the shelfbreak.

[33] Previous studies have calculated f_{SIM} near Denmark Strait and Fram Strait. *Dodd* [2007] reported values typically near ~0.02–0.03 at Denmark Strait, in line with the observations from section 4 of JR105 (Figure 5b). Farther

north at Fram Strait, f_{SIM} are commonly negative (like in the Arctic) and were observed to reach a maximum of ~0.01–0.02 in data from the summer of 1998 [*Meredith et al.*, 2001; *Jones et al.*, 2008]. The JR105 data reveal the importance of melting sea ice to the freshwater composition of the EGC/EGCC system south of Denmark Strait. The meltwater fractions exceed 0.10 south of 63°N, transforming waters of negative f_{SIM} to waters with positive f_{SIM}.

3.3. Meteoric Water

[34] The MW fractions calculated for JR105 (Figure 6) complement the results for SIM and PW discussed above. In general, f_{MW} are greatest at the surface and inshore, and decrease toward the open ocean and deeper waters. This observation could imply two things, either the main source of MW to the EGCC is meltwater runoff from Greenland, thus enhancing the MW fractions observed near the coast, or that the Arctic river component of MW (brought to southeast Greenland via the EGC through Fram Strait) is organized by the wind and currents into a similar distribution. We cannot distinguish between these two MW sources here without additional tracers. As such, we have assumed that runoff from Greenland has the same end-member value as Arctic rivers and precipitation. This is justified by the brief discussion of the isotopic signature of Greenland meltwater in section 3.4 below.

[35] The MW structure that is characteristic of the EGCC is first apparent at JR105 section 4 (Figure 6b), where f_{MW} reach ~0.12 on the inshore side of the jet and decrease offshore. If the inshore enhancement of f_{MW} is primarily due to additional meltwater, it is most likely from the KG fjord region (Figure 1), which is a highly active outlet glacier [*Azetsu-Scott and Tan*, 1997]. This addition of MW to the inshore side of the EGCC would strengthen the cross-shelf density gradient and could play a role in the formation of the EGCC, an observation made previously [*Bacon et al.*, 2002; *Bacon et al.*, 2008]. On the other hand, MW advected inshore due to strong downwelling favorable winds would produce a similar f_{MW} structure and lead to an enhanced cross-shelf density gradient.

[36] Values of f_{MW} are similar at sections 3 and 2 (Figures 6c and 6d), again confined to the near-surface waters. By Cape Farewell, a significant part of the MW signal present farther north is absent (Figure 6e), as was true of the PW signal at this location. The MW component is likely more efficiently mixed into ambient shelf water by the wind as it lies primarily in the surface layer. The higher values seen inshore (near $x = 15$ km) are consistent with the presence of the EGCC, but in a highly mixed state due to the strong winds prior to the sampling. Recall that almost no PW or SIM was present within the coastal current at section 1 (Figures 4e and 5e).

[37] High percentages of MW, $f_{\mathrm{MW}} > 0.10$, have been noted before in the EGC near Denmark Strait [*Jones et al.*, 2008; *Dodd*, 2007] and Fram Strait [*Meredith et al.*, 2001; *Taylor et al.*, 2003]. Closer to the Arctic Ocean, the meteoric water fraction represents more riverine water; for instance *Taylor et al.* [2003] found that in 1998 the dominant source of MW in Fram Strait was Eurasian river runoff, where they differentiated between river types by using barium as an additional tracer. Along southeast Greenland however, the input of glacial meltwater represents a potentially signifi-

cant additional freshwater input, added to the river runoff already present in the EGC.

3.4. Uncertainties

[38] The above freshwater composition analysis of the EGCC, based on equations (1)–(4), was limited to a qualitative description of the relative distributions of PW, SIM, and MW for several reasons. The approach relies on choosing appropriate end-member values, which must reflect the bulk water properties (salinity, oxygen isotope, N-P relationship) of source regions that can vary seasonally and spatially. Previous studies have done sensitivity tests addressing what variable and/or source water elicits the most change in the composition [*Taylor et al.*, 2003; *Bauch et al.*, 1995]. We do not repeat these analyses here for the JR105 data. The largest errors most likely arise in calculating f_{PW} in equation (1), which are on the order of ±10%. This uncertainty comes about through errors in determining the slope and intercept of the AW/PW lines in Table 1 (also see Figure 2), and/or through local processes, such as denitrification or nitrogen fixation, on the Greenland shelves that could modify the nutrient relationships away from the source regions. Possible processes affecting the N-P relationship are discussed in more detail by *Jones et al.* [2003].

[39] Given these bounds on the accuracy of the f_{PW} calculation in equation (1), we can test the sensitivity of the remaining freshwater fractions, f_{MW} and f_{SIM}, to the choice of method used above. We do this by showing the difference between the results as calculated above in equations (2)–(4) versus the results found from a similar, but slightly altered, method. The second method utilizes the same set of equations but replaces δ^{18}O with alkalinity as a tracer of meteoric water. Alkalinity has been used successfully to identify runoff pathways in the Arctic, since the major rivers have been shown to have a unique alkalinity signature, as illustrated previously in Figure 3b [see also *Anderson et al.*, 1994, 2004]. The alkalinity end-members used here (Table 2) are from *Anderson et al.* [2004], although the published range for Arctic rivers is ~800–1400 μmol kg^{-1} [*Jones et al.*, 2008; *Anderson et al.*, 1994]. The alkalinity value for glacial meltwater is uncertain, so again we assume the value is the same as for rivers and precipitation.

[40] Table 3 lists the results of the above comparison in terms of the difference between the calculated f_{MW} and f_{SIM} for each method. We find that the original f_{SIM} values are greater than those found with the second method, while the original f_{MW} are less. Whether this implies that the original method is biased to give slightly higher (lower) fractions of SIM (MW) is an important question. However, the range of mean differences found was only −0.015–+0.036, which is small compared to the limits on the accuracy of calculating f_{PW} discussed above. It is also comparable to the sensitivity analyses of previous studies, on the order of ~5% [*Taylor et al.*, 2003; *Bauch et al.*, 1995].

[41] Numerous other tracers have been utilized in the past to examine Arctic freshwater pathways, including silicate [e.g., *Stefansson*, 1968; *Codispoti and Lowman*, 1973; *Anderson et al.*, 1994], the ratio NO/PO [*Wilson and Wallace*, 1990], PO$_4$* [*Ekwurzel et al.*, 2001], and barium [e.g., *Taylor et al.*, 2003; *Dodd*, 2007]. Adding these tracers

Table 3. Means and Standard Deviations of the Difference (Δ) in f_{MW} and f_{SIM} Using Alkalinity Instead of $\delta^{18}O$ in Equations (2)–(4)[a]

	$(\Delta f_{SIM})_{Alk-O18}$	$(\Delta f_{MW})_{Alk-O18}$
Δ_{mean}	−0.015	0.036
$\Delta_{std.dev.}$	0.03	0.04

[a](Alk-O18) is based on 32 stations, spread over all the JR105 sections, where both tracers were measured.

to the present analysis, however, would introduce more uncertainties since silicate (as does nitrate, phosphate, and barium) levels depend on biological activity, and NO/PO and PO_4* are not suitable for near surface waters where oxygen can be exchanged with the atmosphere.

[42] Without more information on the variability of the EGCC and its freshwater sources, a more quantitative analysis is unwarranted, although several recent studies have begun to make progress in unraveling these variations. *Yamamoto-Kawai et al.* [2008] have shown the importance of using the total dissolved inorganic nitrogen content (DIN), which includes ammonia as opposed to nitrate only, in calculating PW fractions offshore of the Chukchi Sea shelf in the Arctic Ocean. A more complete suite of measurements including total DIN should improve the accuracy of the f_{PW} calculation to better than 10%, as well as account for apparent $f_{PW} > 1.0$ reported in the southern Canada Basin. As noted above, it has also been assumed that meltwater runoff from Greenland, included as meteoric water in this study, has the same end-member values as the river runoff and precipitation parts of MW. A start on resolving this issue comes from examining oxygen isotope measurements collected in the KG fjord glacier system (Figure 1). The 1993 cruise reported by *Azetsu-Scott and Tan* [1997], and the 2004 cruise discussed by *Dodd* [2007], both had extrapolated $\delta^{18}O$ values near −20‰ (with variations of ±1–4‰), which are comparable to the variations seen in MW measurements taken from the Arctic [*Bauch et al.*, 1995]. However, such extrapolations must be viewed with caution, since even comparatively small shifts in salinity due to sea ice processes have the potential to yield very large changes in extrapolated end-member properties at zero salinity.

4. Interannual Variability of the Pacific Water Signal

[43] Once the EGC exits Fram Strait with its PW signature, it carries with it information on aspects of the Arctic Ocean circulation prior to that time. While *Jones et al.* [2003] reported f_{PW}s that were consistently near ~0.9 from 1997 to 1999 in the vicinity of Fram Strait, *Taylor et al.* [2003] noted that data from 1987 showed a maximum of only 0.5 f_{PW}. Recently, *Falck et al.* [2005] showed that the PW fraction decreased dramatically in 2004 north of Greenland, compared to similar sections occupied in 1984, 1990, and 1997. In light of such time-varying PW fractions in the vicinity of Greenland, it is worthwhile to try to link these interannual variations to possible changes in Arctic export pathways.

[44] What controls the amount of Pacific Water present in the EGC? *Steele et al.* [2004] argue that the PW pathways in the Arctic are strongly affected by the Arctic Oscillation (AO), which is defined as the leading mode of an empirical orthogonal function decomposition of the 1000-mb pressure field over the wintertime northern hemisphere (AO data available at http://www.cpc.ncep.noaa.gov/). In particular, during persistent positive AO phases, the anticyclonic Beaufort gyre weakens and shrinks in size, allowing more PW to progress along the boundary to Fram Strait as well as via the Transpolar Drift Stream (see Figure 14 in *Steele et al.* [2004]). When the AO switches to a strongly negative state, the enhanced Beaufort gyre effectively limits the amount of PW that can cross the Arctic basin, and the PW input is either stored in the gyre interior or is drained through the CAA before reaching Fram Strait. These two states of the Arctic Ocean were described in detail by *Proshutinsky and Johnson* [1997], who focused mainly on the surface water circulation and sea ice drift that are linked directly to the atmosphere. In the Arctic, PW is found from the surface to depths of 200 m, so its circulation is directly linked to the atmospheric as well.

[45] Three types of Pacific Water occupy portions of the Arctic Ocean halocline [e.g., *Coachman et al.*, 1975; *Shimada et al.*, 2001; *Steele et al.*, 2004]. Following the nomenclature of *Steele et al.* [2004], these are: summer Bering Sea Water (sBSW), Alaska Coastal Water (ACW), and winter Bering Sea Water (wBSW). These different PW types originate in different regions and are modified by different processes seasonally. They are believed to spread in distinct pathways, though they all are found in water depths less than 200 m and seem to respond to AO forcing [*Steele et al.*, 2004], which allows the use of a more general PW water mass to be considered instead of differentiating between the three types. Importantly, these halocline waters make up part of the subsurface EGC as it exits Fram Strait, with Polar Surface Water in the near surface layer [*Rudels et al.*, 2002]. In the Arctic Ocean, the geographical boundary between the influence of Pacific-origin waters and Atlantic-origin waters is usually defined by the Transpolar Drift Stream, whose location has been shown to respond to changes in the AO index [e.g., *McLaughlin et al.*, 1996]. These shifts in the axis of the Transpolar Drift Stream, and the fact that correlations between the Arctic Ocean circulation above 200 m and the atmosphere reach up to 80% [*Proshutinsky and Johnson*, 1997], strongly suggest that the distribution and advection of PW is causally linked to the varying AO index.

[46] It is worth noting that *Falck et al.* [2005] found no significant correlation between the "disappearance" of PW at Fram Strait in 2004 (when the maximum f_{PW} was 0.20) and the relatively larger percentages found previously, with the AO index. However, their study considered only a small number of sections, limiting their ability to make such a comparison. Since we showed above that there is a strong PW signal in the EGC/EGCC system along southeast Greenland, we can test the relationship between the AO index and the PW signal in the vicinity of Denmark Strait, where there is a relative abundance of nutrient data compared to Fram Strait.

4.1. Calculation of PW Signal

[47] The data for this part of the study are taken from 24 sections that included nitrate, phosphate, temperature,

Table 4. List of Cruises From Which Nutrient Data was Obtained (via Personal Communication or the NODC [*Boyer et al.*, 2006]) for Use in Examining Pacific Water Signals in Section 4[a]

Year	Month	Location[b]	Number of stations (dx)[c]	Vessel (program)[d]	Notes[e]
1984	September	North	4 (40 km)	*Prof. Multanovskyi*	USSR
1987	September	North	5 (20–40 km)	*B. Sæmundsson*	Iceland
1988	September	North	5 (20–40 km)	*B. Sæmundsson*	Iceland
1989	September	North	5 (20–40 km)	*B. Sæmundsson*	Iceland
1990	September	North	5 (20–40 km)	*B. Sæmundsson*	Iceland
1991	September	North	5 (20–40 km)	*B. Sæmundsson*	Iceland
1991	September	Sill	20 (20 km)	*B. Sæmundsson*	Iceland
1993	August	Sill	12 (15 km)	*B. Sæmundsson*	Iceland
1994	September	Sill	10 (20 km)	*B. Sæmundsson*	Iceland
1996	October	North	8 (30 km)	*B. Sæmundsson*	Iceland
1996	November	South	50 (6 km)	*Knorr* (WOCE)	International
1997	August	Sill	11 (10 km)	*Aranda* (VEINS)	Finland
1997	September	Sill	14 (10 km)	*Aranda* (VEINS)	Finland
1997	October	North	8 (30 km)	*B. Sæmundsson*	Iceland
1998	October	North	13 (20 km)	*Polarstern* (VEINS)	*Dodd* [2007]
1998	October	Sill	9 (20 km)	*Polarstern* (VEINS)	*Dodd* [2007]
1998	October	South	10 (20 km)	*Polarstern* (VEINS)	*Dodd* [2007]
1999	September	Sill	3 (25 km)	*B. Sæmundsson*	Iceland
2001	August	Sill	1 (N/A)	*B. Sæmundsson*	Iceland
2002	May	North	10 (30 km)	*Oden*	*Jones et al.* [2008]
2002	May	Sill	6 (30 km)	*Oden*	*Jones et al.* [2008]
2002	May	South	8 (30 km)	*Oden*	*Jones et al.* [2008]
2004	August	North	33 (5 km)	*James Clark Ross*	Sect. 5 in Figure 2.1
2004	August	South	37 (5 km)	*James Clark Ross*	Sect. 4 in Figure 2.1
2004	August	South	19 (5 km)	*James Clark Ross*	Sect. 3 in Figure 2.1
1998	September	Fram Strait	23 (10 km)	*Polarstern* (VEINS)	*Meredith et al.* [2001]
1998	September	75°N	12 (20 km)	*Polarstern* (VEINS)	Germany
1999	September	Fram Strait	16 (15 km)	*Polarstern* (VEINS)	*Taylor et al.* [2003]
1999	October	75°N	6 (20 km)	*Polarstern* (VEINS)	Germany
2002	May	Fram Strait	8 (20 km)	*Oden*	*Jones et al.* [2008]

[a]References are given when available.
[b]Location is relative to the Denmark Strait area (Figure 1) or indicates Fram Strait or 75°N.
[c]This is the number of stations used in the PW_{equiv} calculation and the average horizontal spacing, dx.
[d]WOCE: World Ocean Circulation Experiment.
[e]VEINS: Variability and Exchange in the Nordics Seas.

and salinity measurements. The locations of each cruise are shown in Figure 1b, identified by their proximity to Denmark Strait as either northern (green), sill (red), or southern (blue) sections. They include sections 3–5 of JR105 that were discussed above in detail, and cover the years 1984, 1987–1999, 2002, and 2004. The 2002 data come from a May cruise aboard the *IB Oden*, analyzed by *Jones et al.* [2008]. The 1998 data are from the ARK-XIV2 expedition aboard the *R/V Polarstern*, and have been previously discussed by several authors [*Meredith et al.*, 2001; *Taylor et al.*, 2003; *Dodd*, 2007]. The remaining data come from E. P. Jones (personal communication, 2007) and from the archives of the National Oceanographic Data Center [*Boyer et al.*, 2006; available at http://www.nodc.noaa.gov/]. Most of the northern sections are from Icelandic repeat cruises along the standard Kögur section. Details of each cruise are given in Table 4.

[48] While the vertical and horizontal resolutions of the sections varied (Table 4), they all captured the presence of the EGC (or EGCC in the southern sections) front, with fresher/colder water inshore of the saltier/warmer waters of Atlantic influence. The position of the front is indicated for each section in Figure 1b, which coincides with the location of the maximum equatorward geostrophic velocity, calculated from the θ/S data and referenced to the bottom. In general, the frontal position was located near the shelfbreak north of Denmark Strait, but varied in position near the sill,

either close to the shelfbreak on the Greenland side or in the middle of the strait. An offshore veering of the EGC as it crosses over the sill is commonly observed [e.g., *Hansen and Østerhus*, 2000]. Downstream of the sill, the front shifts inshore again and the EGC splits into the inner shelf EGCC and the shelfbreak EGC.

[49] To quantify the amount of PW present at each section we followed the first step of the freshwater decomposition outlined above, i.e., using equation (1). However, the AW* source line was determined for each section independently before solving equation (1). This was accomplished by fitting a line to the N-P data from each section that had $S > 35$, a proxy for AW. Figure 7 shows the composite nitrate-phosphate relationship for all the Denmark Strait sections (yellow circles), and demonstrates why this extra step was necessary. Without accounting for changes in the AW* source line, the estimated f_{PW}s could be biased. We emphasize, though, that the shifting of the AW* line never exceeded the upper and lower bounds estimated previously from the JR105 data. In essence, this step tries to account for variability in the AW* nutrient relationship, and should be done for the PW line as well. However, since our data are far from the PW source region, it is impossible to derive a PW fit for each year based only on data from that section. We assume therefore that the single PW source line (Figure 7) is satisfactory for all the data, within its estimated upper and lower bounds.
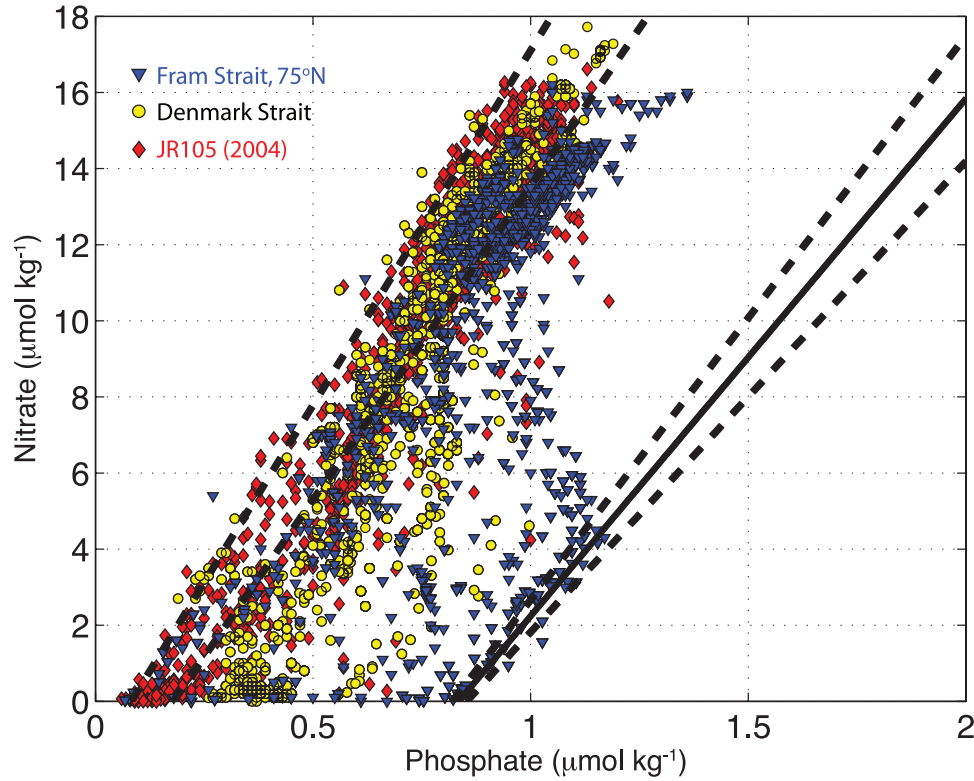
Figure 7. Phosphate versus nitrate values for data from Denmark Strait (yellow circles), Fram Strait and 75°N (blue triangles), and JR105 (red diamonds). AW fits were found for each section between the upper and lower bounds, while the single PW fit was used exclusively (solid black line). Note that these are the same source lines as shown in Figure 2.

[50] Once the f_{PW} is calculated for each section, we then convert it to its freshwater equivalent value

$$f_{PW}^{fresh} = f_{PW}(1 - S_{PW}/S_{AW}) \qquad (5)$$

where S_{PW} and S_{AW} are the salinities of Pacific Water and Atlantic Water respectively (Table 1). The total fresh water equivalent relative to the AW salinity can be calculated as

$$f_{total}^{fresh} = 1 - S_m/S_{AW} \qquad (6)$$

where S_m is the measured salinity. We use these instead of f_{PW} from equation (1) to facilitate comparison with other studies, which report PW freshwater inventories. With these variables defined, we constructed vertical sections of PW freshwater equivalent and total freshwater (FW) content for each year/location.

[51] It is necessary to account for the variations in the spatial coverage of each section, since not all of them crossed completely through the relevant current feature. For example, some of the sections near the sill did not sample the entire EGC, since those transects did not survey all the way to the coast (Figure 1). We account for this by first integrating f_{PW}^{fresh} and f_{total}^{fresh} in the vertical (0–200 m) to get column inventories of PW and FW equivalent (in meters). Next we integrate these in the horizontal to get an area of PW and FW equivalent (m^2). These values were then normalized by dividing by the horizontal extent of the

current feature that was captured in the section, either the EGC in the north and sill sections, or the EGCC in the southern sections. The final normalized PW and FW equivalent inventories are thus defined as

$$PW_{equiv} = \frac{1}{L} \iint_{dx,0-200m} f_{PW}^{fresh} dzdx \qquad (7)$$

$$FW_{equiv} = \frac{1}{L} \iint_{dx,0-200m} f_{total}^{fresh} dzdx \qquad (8)$$

where L is the estimated horizontal extent of the current (in meters). This provides a single value that can be meaningfully compared between each year/section, reflecting the amount of PW or FW present. The one exception to this is the 2001 cruise in the sill region, which contained only a single station. For that station, we assumed the data represented a horizontal extent comparable to the station spacing of a similar cruise to that area undertaken in 1999 (see Table 4), i.e., $L \sim 25$ km. This normalization introduces the largest uncertainties in the sill sections, since these commonly did not capture the entire EGC. Therefore these PW_{equiv} values have the largest error bars.

[52] Figure 8 displays the results of the calculation for PW_{equiv}, with a separate curve for each of the three groups of sections (north of the Denmark Strait sill, near the sill, and south of the sill). The range over all years is 0.5–3.5 m,
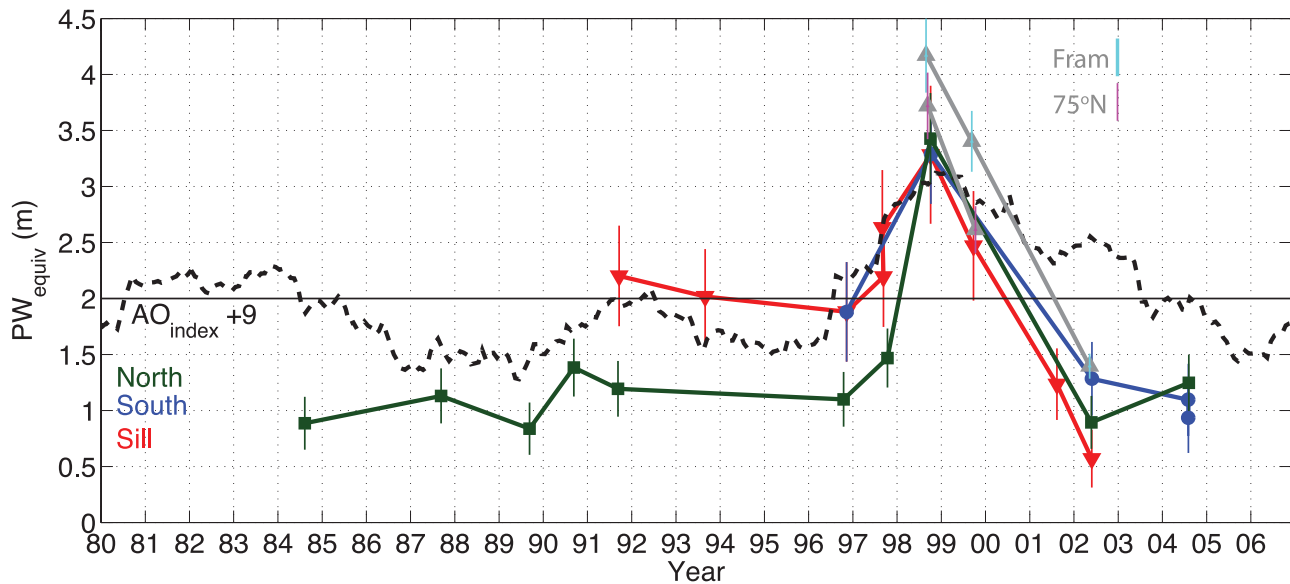
Figure 8. Normalized Pacific Water freshwater equivalent inventory, PW_{equiv} (m), as a function of time. The 24 sections from the Denmark Strait area are grouped by location as either northern (green squares), sill (red diamonds), or southern (blue circles). Five sections taken from north of Denmark Strait (Fram Strait and 75°N) are shown in gray for comparison. The black dashed line is the 3-year running mean of the wintertime Arctic Oscillation index ($AO_{index}+9$), lagged 9 years, with zero indicated by the black solid line.

which is significantly greater than the estimated uncertainty of each value. The uncertainties (shown as error bounds in Figure 8) are found by combining an estimate of the standard error with the initial 10% uncertainty assumed in calculating f_{PW} in equation (1). The standard error accounts for the synoptic variability, such as observed in years in which two or more sections were taken close to each other in time and location (e.g., 1997, 2004 in Figure 8). An additional 10% error is factored in for the sill section values to represent the added uncertainty in estimating L at those sections, as discussed above. The fact that the temporal trends in PW_{equiv} from different locations covary supports the robustness of the method and the high quality of the data.

[53] The most striking feature in Figure 8 is the large increase in PW_{equiv} observed in the late 1990s, where it reached values of $3.2-3.4 \pm 0.5$ m. The subsequent dramatic decrease supports the observations of *Falck et al.* [2005] at Fram Strait, where a correspondingly large decrease in PW abundance was found in 2004. Several additional sections from the 2002 *Oden* cruise, located between Fram Strait and Denmark Strait, also showed similarly low proportions of PW present [*Jones et al.*, 2008]. To make sure the large pulse in Figure 8 was not predominantly the result of a single anomalous cruise in Denmark Strait in 1998, we calculated PW_{equiv} and FW_{equiv} from five additional sections occupied north of Denmark Strait in the years 1998, 1999, and 2002. Three of these additional sections come from Fram Strait (the 1998 value is from the same cruise as the 1998 Denmark Strait sections), and the other two were occupied across the EGC at 75°N (1998, 1999). See Table 4 for cruise details for each section.

The N-P relationships of these additional data are displayed in Figure 7 and indicate the presence of some "pure" PW at Fram Strait.

[54] The PW_{equiv} values from these northern sections are plotted in Figure 8 (gray lines) in addition to the Denmark Strait data, and match up well with the observations from farther south. Note that the transit time from Fram Strait to Denmark Strait is fairly quick for waters in the EGC, taking on average 6–9 months (based on an average speed of ~0.1 m s^{-1}). This is short compared to residence times estimated for the Arctic Ocean, which are on the order of a decade [e.g., *Schlosser et al.*, 1994; *Ekwurzel et al.*, 2001; *Steele et al.*, 2004]. The exact timing is likely more complicated, since for example, part of the EGC feeds the gyre situated over Belgica Bank that forms the Northeast Water Polynya [*Budeus et al.*, 1997; *Falck*, 2001]. This may act to delay the propagation of the PW signal down the coast, as would any recirculation of the EGC into the Greenland Sea, such as into the Jan Mayen Current or East Icelandic Current.

[55] Figure 8 supports the notion that the PW signal in the EGC was indeed enhanced in the late 1990s. The fact that the PW fraction generally decreases from Fram Strait to Denmark Strait in a given year (e.g., 1998, 2002) is evidence that the method produces a meaningful signal, and that PW is being diluted and redistributed as it traverses southward along the Greenland shelf. The trend of lower PW_{equiv} in the northern Denmark Strait sections compared to the sill sections in the years 1991, 1993, 1996, and 1997 possibly reflects the higher uncertainty in the sill section values, but also the potential that part of the EGC is offshore of the northern sections as it approaches Denmark Strait. This
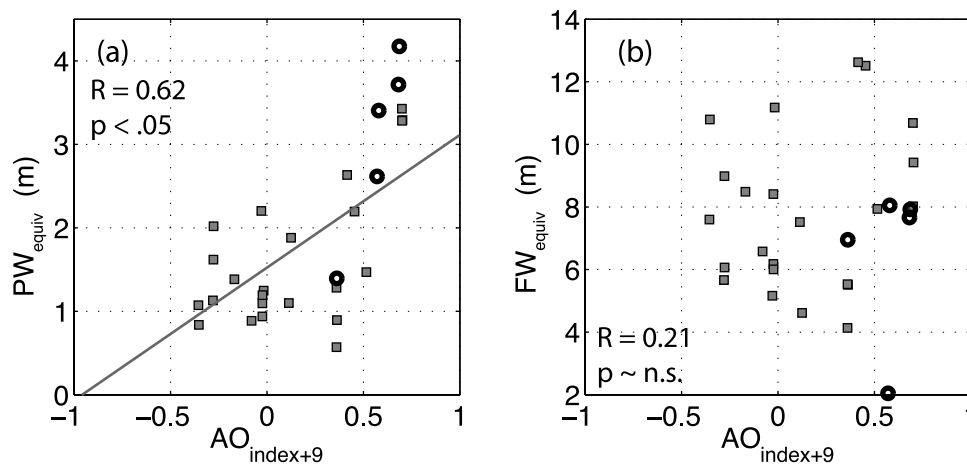
Figure 9. (a) Correlation of the normalized PW inventory, PW_{equiv} (m), from the Denmark Strait sections (gray squares) and the 9-year lagged wintertime AO index. The best fit regression line to these data is shown in gray. Black circles show the corresponding values for the Fram Strait and 75°N sections. Correlation coefficients (R) and the significance of the correlation (p) are shown. (b) Same as in Figure 9a except for the normalized FW inventory, FW_{equiv} (m), which showed no significant correlation.

would result in lower values for the northern sections. It might also be due to a sampling bias in the northern sections, which during this time period, had the lowest spatial resolution and may not have captured the full PW signal. The normalization in equations (7) and (8) would not account for this type of error.

4.2. Link to the Arctic Oscillation

[56] We now examine the correlations between the PW signals in Figure 8 and the wintertime Arctic Oscillation. The 3-year running mean AO index, lagged by 9 years, is included in Figure 8. One immediately sees the intriguing relationship between the lagged AO and the trends in PW_{equiv}. In particular, the AO displayed a similar sharp peak roughly a decade earlier. To investigate this more quantitatively, we linearly regress the values of the AO index with different variables associated with the EGC. Figure 9 shows the results of these correlations. The maximum correlation between PW_{equiv} and the AO was found to be $R = 0.62$ with a lag of 9 years. This is significant at the 95% level (p value) using an effective number of degrees of freedom of 15. No significant correlation was found between the AO index (at any lag) and the FW_{equiv} values; Figure 9b shows these two variables plotted against each other for the AO index plus 9 years. The lack of significant correlation between the freshwater content of the EGC and the AO index is most likely caused by local and seasonal effects that change the amount of freshwater stored in the water column. The major process is sea ice melt during the warmer months, which greatly lowers the salinity of surface waters.

[57] We believe that the significant correlation between the PW_{equiv} and the lagged AO index reflects a difference in the pathways and mixing history of the Pacific Water resulting from changes in the predominant atmospheric forcing of the Arctic, as discussed above (see Figure 14 in *Steele et al.* [2004]). In the positive AO state (weak Beaufort gyre), there is a more direct route for Pacific-origin water to enter Fram Strait via the boundary current and transpolar drift, and hence one would expect a stronger

presence of PW in the EGC (larger values of PW_{equiv}). In the negative AO state (stronger Beaufort gyre), *Steele et al.* [2004] argue that more of the Pacific-origin water exits the Arctic through the Canadian Arctic Archipelago, implying the EGC would receive less PW (smaller values of PW_{equiv}). On the other hand, the results of the linear regression do not rule out a threshold behavior, whereby during high AO states a significant amount of PW is released, while during low to neutral AO states no clear signal appears.

[58] Why is the lag 9 years? Numerous studies have estimated residence times of different water types in the Arctic. *Ekwurzel et al.* [2001] found tracer-derived ages of approximately 8 years for waters just north of Greenland that contained significant Pacific Water fractions. The residence time of waters in the upper 300 m of the Canada Basin, which include the PW layer, was estimated to be 10.8 ± 3.8 years by *Yamamoto-Kawai et al.* [2008], who based their calculations on a freshwater decomposition similar to that outlined above. These times are generally consistent with the lag computed from Figure 9a. However, the different pathways of PW described above likely vary in response to the AO. *Steele et al.* [2004] calculated transit times of PW from the Bering Sea to north of Greenland that range from roughly 5 years in the positive AO state, to approximately 10 years in the negative AO state. In reality, the timing for Pacific-origin water to appear in the EGC is complex and likely relies on several factors, including storage in the Beaufort gyre and the state of the boundary current. Nonetheless, in an average sense, the lag of 9 years computed here is plausible in light of what is presently known about residence times in the western Arctic. What our results do not shed light on is whether, in years of low PW content in the EGC, there is a corresponding increase in PW discharge to the CAA.

5. Conclusions and Summary

[59] Using a suite of tracers collected in summer 2004, it has been shown that the waters of the southeast Greenland shelf and slope are partially of Arctic origin. Significant

amounts of PW were found in the EGC and the EGCC from Denmark Strait south to 63°N. This PW signal in the EGCC supports the previously expressed notion that the current is an inner-shelf branch of the EGC. By Cape Farewell, however, no Pacific Water was observed, suggesting that by this latitude either wind mixing or cross-frontal exchange with offshore Atlantic-origin water had destroyed the Pacific signature. In addition to its link to the EGC, the EGCC is modified by the input of meltwater runoff from Greenland and the melting of sea ice along its path. The use of oxygen isotope data as a tracer, combined with the nitrate-phosphate results, allowed the quantification of these additional sources of freshwater. Fractions of sea ice melt and meteoric water in the EGCC (including meltwater runoff from Greenland, together with precipitation and river runoff from the Arctic) increased southward to maximum values of 10–12%.

[60]   The spatial distribution of the Pacific Water, sea ice melt, and meteoric water signals showed a structure closely linked to the velocity and salinity fields of the EGCC. In particular, the high-resolution station spacing during the 2004 cruise showed that each significant PW fraction signal was associated with a jet feature, was enhanced beneath the surface layer, and was eroded in the upper core of the jet. Sea ice melt and meteoric waters also showed variability on small spatial scales: sea ice melt was surface-trapped and influenced strongly by the wind, while meteoric water resided in the surface layer as well and was generally more pronounced toward the coast. Negative sea ice melt fractions observed in waters north of Denmark Strait reflect their Arctic origin and imply that sea ice was formed from them at some point during the previous winter(s).

[61]   By examining historical data collected near Denmark Strait, it was shown that the PW signal observed in 2004 was in fact weakened when compared with previous years. The historical data, extending from 1984–2004, indicated large interannual variations in the amount of Pacific Water present in the EGC/EGCC system, with a pronounced maximum during the late 1990s. It was argued that this trend is likely linked to the circulation of the Arctic Ocean, where the Pacific Water spreads in pathways controlled to a large degree by the Arctic Oscillation (AO). We found that the PW signals near Denmark Strait are significantly correlated with the AO, with a 9-year time lag. Such a lag agrees qualitatively with previous estimates of residence times in the Arctic, which range from 5 to 11 years. However, no significant correlation was found between the total freshwater content and the AO, suggesting that local and seasonal processes dominate the salinity field over any propagating signal from the Arctic.

References

Anderson, L. G., G. Bjork, O. Holby, E. P. Jones, G. Kattner, K. P. Koltermann, B. Liljebad, R. Lindegren, B. Rudels, and J. Swift (1994), Water masses and circulation in the Eurasian Basin: Results from the *Oden 91* expedition, *J. Geophys. Res.*, 99, 3273–3283.

Anderson, L. G., S. Jutterstrom, S. Kaltin, E. P. Jones, and G. Bjork (2004), Variability in river runoff distribution in the Eurasian Basin of the Arctic Ocean, *J. Geophys. Res.*, 109, C01016, doi:10.1029/2003JC001773.

Azetsu-Scott, K., and F. C. Tan (1997), Oxygen isotope studies from Iceland to an East Greenland Fjord: Behavior of glacial meltwater plume, *Mar. Chem.*, 56, 239–251.

Bacon, S., G. Reverdin, I. G. Rigor, and H. M. Smith (2002), A freshwater jet on the east Greenland shelf, *J. Geophys. Res.*, 107(C7), 3068, doi:10.1029/2001JC000935.

Bacon, S., P. G. Myers, B. Rudels, and D. A. Sutherland (2008), Accessing the inaccessible: Buoyancy-driven coastal currents on the shelves of Greenland and eastern Canada, in *Arctic-Subarctic Ocean Fluxes: Defining the Role of the Northern Seas in Climate*, edited by R. Dickson, J. Meincke, and P. Rhines, 738 pp., Springer, New York.

Bauch, D., P. Schlosser, and R. G. Fairbanks (1995), Freshwater balance and the sources of deep and bottom waters in the Arctic Ocean inferred from the distribution of $H_2^{18}O$, *Prog. Oceanogr.*, 35, 53–80.

Boyer, T. P., J. I. Antonov, H. E. Garcia, D. R. Johnson, R. A. Locarnini, A. V. Mishonov, M. T. Pitcher, O. K. Baranova, and I. V. Smolyar (2006), World Ocean Database 2005, in *NOAA Atlas NESDIS 60*, edited by S. Levitus, 190 pp., U.S. Government Printing Office, Washington, D. C.

Budeus, G., W. Schneider, and G. Kattner (1997), Distribution and exchange of water masses in the Northeast Water Polynya, *J. Mar. Syst.*, 10, 123–138.

Cavalieri, D., C. Parkinson, P. Gloerson, and H. J. Zwally (2005), *Sea Ice Concentrations From Nimbus-7 SMMR and DMSP SSM/I Passive Microwave Data, 2001–2004*, National Snow and Ice Data Center, Boulder, Colo.

Centurioni, L. R., and W. J. Gould (2004), Winter conditions in the Irminger Sea observed with profiling floats, *J. Mar. Res.*, 62, 313–336.

Coachman, L. K., K. Aagaard, and R. B. Tripp (1975), *Bering Strait: The Regional Physical Oceanography*, 172 pp., Univ. Washington Press, Seattle, Wash.

Codispoti, L. A., and D. Lowman (1973), A reactive silicate budget for the Arctic Ocean, *Limnol. Oceanogr.*, 18, 448–456.

Cooper, L. W., T. E. Whitledge, J. M. Grebmeier, and T. Weingartner (1997), The nutrient, salinity, and stable oxygen isotope composition of Bering and Chukchi Seas waters in and near Bering Strait, *J. Geophys. Res.*, 102, 12,563–12,574.

Dickson, R., B. Rudels, S. Dye, M. Karcher, J. Meincke, and I. Yashayaev (2007), Current estimates of freshwater flux through Arctic and subarctic seas, *Prog. Oceanogr.*, 73, 210–230.

Dodd, P. (2007), The freshwater transport of the East Greenland Current, M.S. thesis, Univ. East Anglia, Norwich, UK.

Ekwurzel, B., P. Schlosser, R. A. Mortlock, and R. G. Fairbanks (2001), River runoff, sea ice meltwater, and Pacific water distribution and mean residence times in the Arctic Ocean, *J. Geophys. Res.*, 106, 9075–9092.

Falck, E. (2001), Contribution of waters of Atlantic and Pacific origin in the Northeast Water Polynya, *Polar Res.*, 20, 193–200.

Falck, E., G. Kattner, and G. Budeus (2005), Disappearance of Pacific Water in the northwestern Fram Strait, *Geophys. Res. Lett.*, 32, L14619, doi:10.1029/2005GL023400.

Gordon, L. I., J. C. Jennings, A. A. Ross, and J. M. Krest (1993), A suggested protocol for continuous flow automated analysis of seawater nutrients (phosphate, nitrate, nitrite, and silicic acid) in the WOCE Hydrographic Program and the Joint Global Ocean Fluxes Study, WOCE Hydrogr. Program Off., Woods Hole, Mass.

Hansen, B., and S. Østerhus (2000), North Atlantic-Nordic Seas exchanges, *Progr. Oceanogr.*, 45, 109–208.

IOC, IHO, and BODC (2003), Centenary Edition of the GEBCO Digital Atlas, on behalf of the Intergovernmental Oceanographic Commission and the International Hydrographic Organization as part of the General Bathymetric Chart of the Oceans [CD-ROM], British Oceanographic Data Centre, Liverpool, U. K.

Jones, E. P., L. G. Anderson, and J. H. Swift (1998), Distribution of Atlantic and Pacific waters in the upper Arctic Ocean: Implications for circulation, *Geophys. Res. Lett.*, 25, 765–768.

Jones, E. P., J. H. Swift, L. G. Anderson, M. Lipizer, G. Civitarese, K. K. Falkner, G. Kattner, and F. McLaughlin (2003), Tracing Pacific water in the North Atlantic Ocean, *J. Geophys. Res.*, 108(C4), 3116, doi:10.1029/2001JC001141.

Jones, E. P., L. G. Anderson, S. Jutterström, and J. H. Swift (2008), Sources and distribution of fresh water in the East Greenland Current, *Prog. Oceanogr.*, doi:10.1016/j.pocean.2007.06.003.

Lentz, S. J., and J. Largier (2006), The influence of wind forcing on the Chesapeake Bay buoyant coastal current, *J. Phys. Oceanogr.*, 36, 1305–1316.

Malmberg, S.-A., H. G. Gade, and H. E. Sweers (1967), Report on the second joint Icelandic-Norwegian expedition to the area between Iceland

and Greenland in August–September 1965, *NATO Subcomm. on Oceanogr. Res. Tech. Rep., 41*, Irminger Sea Project, 44 pp., Reykjavik, Iceland.

McLaughlin, F. A., E. C. Carmack, R. W. MacDonald, and J. K. Bishop (1996), Physical and geochemical properties across the Atlantic/Pacific water mass front in the southern Canadian Basin, *J. Geophys. Res., 101*, 1183–1197.

Meredith, M., K. Heywood, P. Dennis, L. Goldson, R. White, E. Farbach, U. Schauer, and S. Osterhaus (2001), Freshwater fluxes through the western Fram Strait, *Geophys. Res. Lett., 28*, 1615–1618.

Östlund, H. G., and G. Hut (1984), Arctic Ocean water mass balance from isotope data, *J. Geophys. Res., 89*, 6373–6381.

Pickart, R. S., D. J. Torres, and P. S. Fratantoni (2005), The East Greenland spill jet, *J. Phys. Oceanogr., 35*, 1037–1053.

Proshutinsky, A. Y., and M. A. and Johnson (1997), Two circulation regimes of the wind-driven Arctic Ocean, *J. Geophys. Res., 102*, 12,493–12,514.

Rudels, B., E. Fahrbach, J. Meincke, G. Budeus, and P. Erikson (2002), The East Greenland Current and its contribution to the Denmark Strait Overflow, *ICES J. Mar. Sci., 59*, 1133–1154.

Schlosser, P., D. Bauch, R. Fairbanks, and G. Bonisch (1994), Arctic river-runoff: Mean residence time on the shelves and in the halocline, *Deep Sea Res. Part A, 41*, 1053–1068.

Serreze, M. C., A. P. Barrett, A. G. Slater, R. A. Woodgate, K. Aagaard, R. B. Lammers, M. Steele, R. Moritz, M. Meredith, and C. M. Lee (2006), The large-scale freshwater cycle of the Arctic, *J. Geophys. Res., 111*, C11010, doi:10.1029/2005JC003424.

Shimada, K., E. C. Carmack, K. Hatakeyama, and T. Takizawa (2001), Varieties of shallow temperature maximum waters in the western Canadian Basin of the Arctic Ocean, *Geophys. Res. Lett., 28*, 3441–3444.

Steele, M., J. Morison, W. Ermold, I. Rigor, M. Ortmeyer, and K. Shimada (2004), Circulation of summer Pacific halocline water in the Arctic Ocean, *J. Geophys. Res., 109*, C02027, doi:10.1029/2003JC002009.

Stefansson, U. (1968), Dissolved nutrients, oxygen, and water masses in the Northern Irminger Sea, *Deep Sea Res., 15*, 541–575.

Sutherland, D. A., and C. Cenedese (2008), Laboratory experiments on the interaction of a buoyant coastal current with a canyon: Application to the East Greenland Current, *J. Phys. Oceanogr., 39*, 1258–1271.

Sutherland, D. A., and R. S. Pickart (2008), The East Greenland Coastal Current: Structure, variability, and forcing, *Prog. Oceanogr.*, doi:10.1016/j.pocean.2007.09.006.

Taylor, J. R., K. K. Falkner, U. Schauer, and M. Meredith (2003), Quantitative considerations of dissolved barium as a tracer in the Arctic Ocean, *J. Geophys. Res., 108*(C12), 3374, doi:10.1029/2002JC001635.

Wilkinson, D., and S. Bacon (2005), The spatial and temporal variability of the East Greenland Coastal Current from historic data, *Geophys. Res. Lett., 32*, L24618, doi:10.1029/2005GL024232.

Wilson, C., and D. W. R. Wallace (1990), Using the nutrient ratio NO/PO as a tracer of continental shelf waters in the Central Arctic Ocean, *J. Geophys. Res., 95*, 22,193–22,208.

Yamamoto-Kawai, M., F. A. McLaughlin, E. C. Carmack, S. Nishino, and K. Shimada (2008), Freshwater budget of the Canada Basin, Arctic Ocean, from salinity, δ^{18}O, and nutrients, *J. Geophys. Res., 113*, C01007, doi:10.1029/2006JC003858.

————————————

K. Azetsu-Scott and E. Peter Jones, Bedford Institute of Oceanography, 1 Challenger Drive, P.O. Box 1006, Dartmouth, NS B2Y 4A2, Canada.

A. Jane Eert, Oceanografix, 368 Millstream Lake Road, Victoria, BC V9B 6E9, Canada.

J. Olafsson, University of Iceland and Marine Research Institute, Skulagata 4, P.O. Box 1390, IS 121, Reykjavik, Iceland.

R. S. Pickart, Department of Physical Oceanography, Woods Hole Oceanographic Institution, MS #21, Woods Hole, MA 02543, USA.

D. A. Sutherland, MIT/WHOI Joint Program, Clark 330, MS #21, Woods Hole, MA 02543, USA. (dsutherland@whoi.edu)